Observational evidence of interaction between Equatorial Plasma Bubble, Medium-scale Traveling Ionospheric Disturbances, and Midnight Brightness Wave at low latitudes

C. A. O. B. Figueiredo[1], C. M. Wrasse[1], H. Takahashi[1], Y. Otsuka[2], K. Shiokawa[2], R. A. Buriti[3], I. Paulino[3], D. Barros[1]

[1] Instituto Nacional de Pesquisas Espaciais, São José dos Campos, Brazil.
[2] Institute for Space-Earth Environmental Research, Nagoya University, Nagoya, Japan.
[3] Unidade acadêmica de física, Universidade Federal de Campina Grande, Campina Grande, Brazil.

Corresponding author: Cosme A. O. B. Figueiredo (cosme.figueiredo@inpe.br, anagetinga@gmail.com)

Key Points:

- Rare interaction between plasma bubbles, medium-scale traveling ionospheric disturbances, and midnight brightness wave was observed at low latitudes.
- Equatorial plasma bubbles tilted, narrowed, and grew after the medium-scale traveling ionospheric disturbances crossed them.
- Interaction between equatorial plasma bubbles and midnight brightness wave caused intensification of the plasma density at the edge of the plasma bubble.

Abstract

An interesting interaction between equatorial plasma bubbles (EPBs), medium-scale traveling ionospheric disturbance (MSTID), and midnight brightness wave (MBW) were observed at Cachoeira Paulista, Brazil (22.7°S, 45.0°W, magnetic dip latitude ~20°S) by all-sky images of OI 630 nm emission, on the night of September 17-18, 2015. The EPBs were observed moving eastward while the MSTID propagated northwestward with the wavefront aligned to southwest-northeast. The MBW was observed propagating to south-southwest. After interaction with MSTIDs, the EPBs tilted and became larger and narrower. This effect could be associated with the **E**x**B** drift and also with changes in the neutral wind. Furthermore, the MBW also interacted with EPB and filled the EPB edge with plasma.

Plain Language Summary

Equatorial plasma bubbles (EPBs), medium-scale traveling ionospheric disturbances (TIDs), and midnight brightness waves (MBWs) are phenomena that have been studied individually over several decades. Recently, collapse and shrinking of EPBs has become a subject of interest of the scientific community, due to observations that EPB-TID interaction results in EPB disappearance. We report an interesting and a rare observation of EPBs, MSTID, and MBW using an All-Sky airglow imager at Cachoeira Paulista, Brazil (22.7°S, 45.0W, magnetic dip latitude ~20°S, referring to 2015) on the night of September 17-18, 2015. Interaction with the MSTIDs caused the EPBs to tilt, grow, and to become narrower, but did not disappear. Subsequently, the MBW interacted with the EPB and filled the EPB edge with plasma. This effect could be associated with **E**x**B** drift and also with changes in the neutral wind.

Introduction

Equatorial plasma bubbles (EPBs) are electron density depletions that occur in Earth's ionosphere with a latitudinal dimension of hundreds to thousands of kilometers (e.g., Barros et al., 2018; Clemesha, 1964; Kelley, 2009; Sobral et al., 1980; Takahashi et al., 2015). The most accepted mechanism of EPBs is the Rayleigh-Taylor instability (RTI) associated with layer uplift

of the F layer due to the **E**×**B** drift (Rishbeth, 2000). The RTI theory requires perturbation in the bottom side of the F layer to trigger the EPBs (e.g., Abdu et al., 2015; Haerendel, 1973; Kelley, 2009; Paulino et al., 2011; Tsunoda, R.T., 2010; Vadas et al., 2009).

MSTIDs are understood as the manifestation of gravity wave propagation in the ionosphere (Hines, 1960; Hooke, 1968). MSTIDs can have horizontal wavelengths from hundreds to thousands of kilometers (e.g., Figueiredo et al, 2018a; Hunsucker, 1982). The mechanism of generation of MSTIDs has been proposed to include polarization electric field in addition to the classical theory for gravity waves (e.g., Miller et al., 1997; Kelley & Miller, 1997). Some observations have shown that MSTIDs propagated northwestward in the Southern hemisphere (e.g., Amorim et al., 2011; Figueiredo et al., 2018b) and southwestward in the northern hemisphere (e.g., Otsuka et al., 2012). They were generated by well-known Perkins and E -F layers coupling instability (e.g., Yokoyama and Hysell, 2010). Also, MSTIDs have been observed propagated to other directions as well (Paulino et al., 2016, Figueiredo et al., 2018b).

Recent reports of observations and numerical simulations of medium-scale traveling ionospheric disturbances (MSTIDs) outside the equatorial region suggest that MSTIDs could seed plasma bubbles (e.g., Miller et al, 2009; Krall et al, 2011; Takahashi et al., 2018).

Another type of traveling ionospheric disturbance is known as the midnight brightness wave (MBW) (e.g., Fukushima et al., 2017). MBW is the optical signature of a midnight temperature maximum (MTM) in which the neutral temperature increases by between 50 and 200 K near local midnight (e.g., Figueiredo et al., 2017; Mesquita et al., 2018 and references therein). The MBW leads an increase in OI 630 nm intensity, and then propagates to the poles (e.g., Burnside et al., 1981; Colerico et al., 1996, Fukushima et al., 2017). The midnight pressure bulge, associated with MTM, reverses the meridional wind's direction from equatorwar to poleward (Colerico et al., 1996; Herrero et al., 1993). Consequently, poleward wind moves the F layer down along the magnetic field lines, increasing the intensity of the OI 630 nm emission rates (Link & Cogger, 1988).

EPBs, TIDs, and MBW are phenomena that have been individually studied over several decades

(e.g., Otsuka et al., 2012; Shiokawa et al., (2015); and Narayanan et al., 2016). Recent works have reported that interactions between EPB/TIDs produce collapse and/or shrinkage (Otsuka et al., 2012, Shiokawa et al., 2015, and Narayanan et al., 2016). The main physical mechanisms associated with the plasma bubble disappearance after the EPB/MSTID interaction is the MSTID polarization electric field and the F-region dynamo of the ionospheric/thermospheric waves (Otsuka et al., 2012; Shiokawa et al. 2015).

In this paper, we report an interaction between EPB, MSTID, and MBW which does not result in plasma bubbles disappearance. We observed that plasma bubbles tilted, grew along the magnetic field lines, and became narrower. Enhancement in brightness at their edges after interaction with MSTID and MBW was observed as well. Furthermore, we discuss some physical ionospheric processes required for explaining EPBs non-disappearance after EPB/MSTID and EPB/MBW interactions, which may lead to a better understanding of the equatorial ionosphere.

Observations and results

The All-Sky imager installed at Cachoeira Paulista, Brazil (22.7°S, 45.0W°, magnetic coordinates: 20.4°S, 21.4° E; magnetic coordinates are for 2015) operates with two optical filters: OH Meinel bands and OI 630 nm. It has a fisheye lens with 180° field of view, and a CCD camera with a resolution of 1024x1024 pixels. OI 630 nm images are captured approximately every 110 seconds with an exposure time of 90 seconds.

Figure 1 shows a sequence of detrended OI 630 nm images, captured between 01:57 and 05:48 UT (local time (LT): GMT - 3 hours) of September 17-18, 2015. Detrended images were obtained by subtracting 1-hour running-average images from the original images (Otsuka et al., 2012). The plasma bubbles are indicated by red arrows and propagated north-eastward with a horizontal drift of ~68 m/s. The MSTID wavefronts (indicated by white arrows) were southwest-northeast aligned and propagated northeastward from 01:57 to 04:08 UT with horizontal phase speed of ~135 m/s. Finally, a bright region is observed propagating south-southwest, indicated by blue arrows, with velocity of ~ 131 m/s, between 03:48 and 05:48 UT. The smooth and static region seen in the southwest portion of the image is due to contamination from city lights.

117

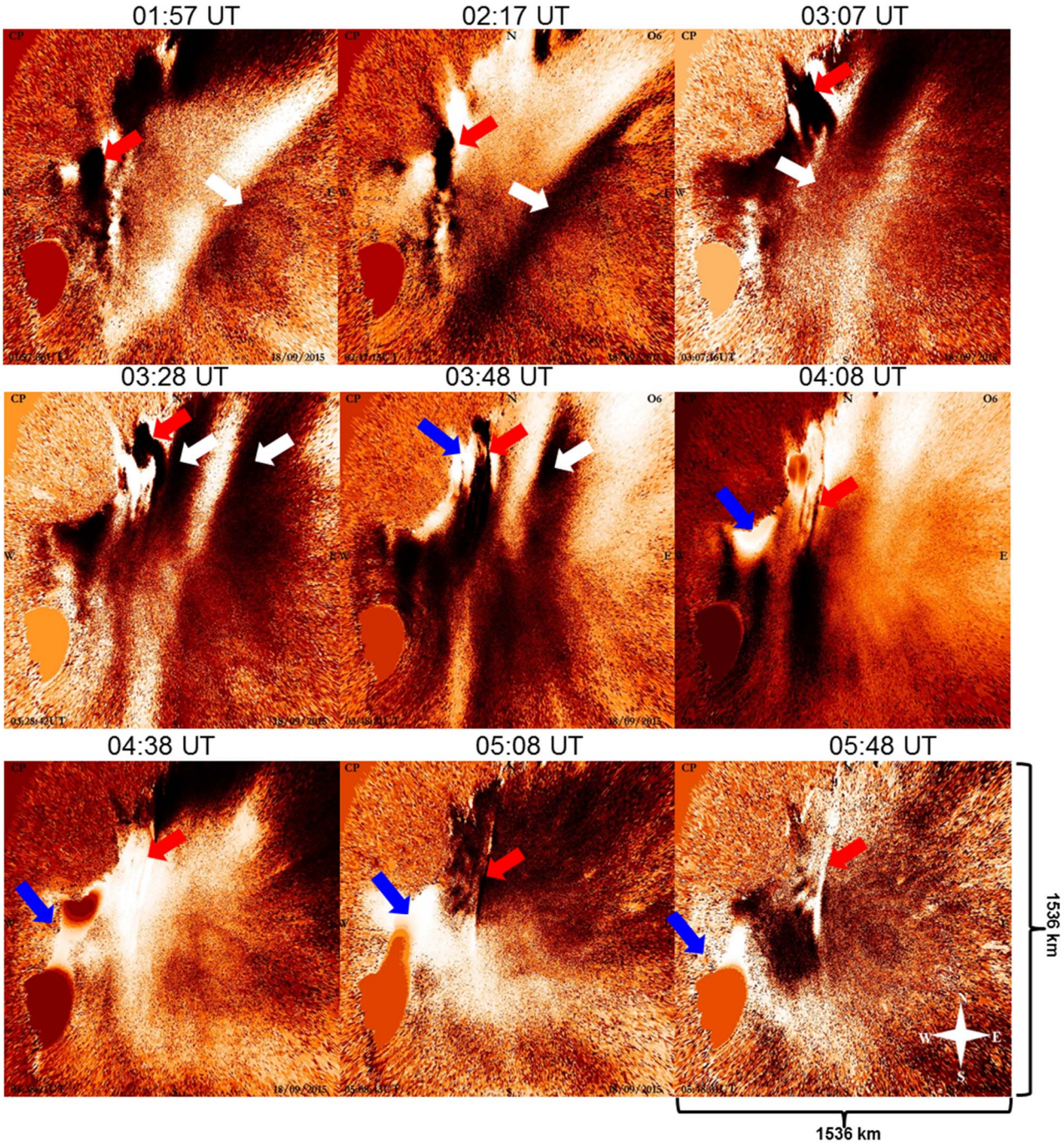

118

119 Figure 1 – Detrended unwarped all-sky images of the OI 630 nm emission observed at Cachoeira
120 Paulista, Brazil, between 01:57 and 05:48 UT. The red arrows indicate depletions associated with
121 EPB, the blue arrows indicate the MBW, and the white arrows indicate the MSTID. Detrended
122 images are obtained by subtracting 1-hour running-average images following the approach
123 described by Otsuka et al., (2012). Trees near the observatory prevent visibility of the sky in the

upper left corner of the image.

The EPBs propagate to the northeast, from ~ 01:57 to 02:17 UT, without a change in their structures. However, at 03:07 UT, the EPBs interacts with the MSTID, then the EPBs tilts, grows latitudinally, and moves slowly westward. The MSTID left the imager´s field of view after 04:25 UT. Next, at 03:48 UT, in the upper left corner of the image, a bright region with higher intensity than the background level appears propagating to south-southwest. The bright region interacts with the EPBs, which become brighter while remaining tilted and narrowed until 06:30 UT (not shown). An animation of Figure 1 is available through the supporting information related to this article, see Movie S1.

To investigate the bright region that propagates southwest, Figure 2 shows (a) an airglow image measured by an all-sky imager; as well as the neutral wind (b and c) components and (d) temperature measured by the Fabry-Perot interferometer (FPI) at São João do Cariri (7.4°S, 36.5°W, magnetic coordinates: 12°S; 33°E; for 2015). Details about FPI and data analysis methodology have been published elsewhere (Makela et al., 2009, and Meriwether et al., 2011). The FPI measures Doppler shift and broadening of the OI 630 nm emission line with an elevation angle of 45° at four cardinal directions (N, S, E, W) and zenith. In Figure 2, it will be noticed that the zonal (b) and meridional (c) components of the thermospheric wind changed their flow direction at 02:00 UT. The zonal component changes from east to west and the meridional component from equatorward to the poleward. Moreover, the neutral temperature (d) increased when compared to the neutral temperature of International Reference Ionosphere (IRI) 2016 model (Bilitza et al., 2017). The IRI 2016 neutral temperature was matched (21:00–21:30 UT) with the observed temperature by applying a constant offset, as described by Meriwether et al. (2011). These characteristics of neutral wind and temperature are the signature of the midnight temperature maximum (Figueiredo et al., 2017).

Figure 2a shows a snapshot of the OI 630 nm all-sky image at São João do Cariri at 03:01 UT. The bright region indicated by a blue arrow is the optical signature of an MTM, which propagates south-southwest, which is also known as a midnight brightness wave (Colerico et al., 1996). Figure 1 shows an MBW (blue arrows), which was also observed at São João do Cariri. A

short movie of the São João do Cariri's images is shown in the supplementary Movie S2.

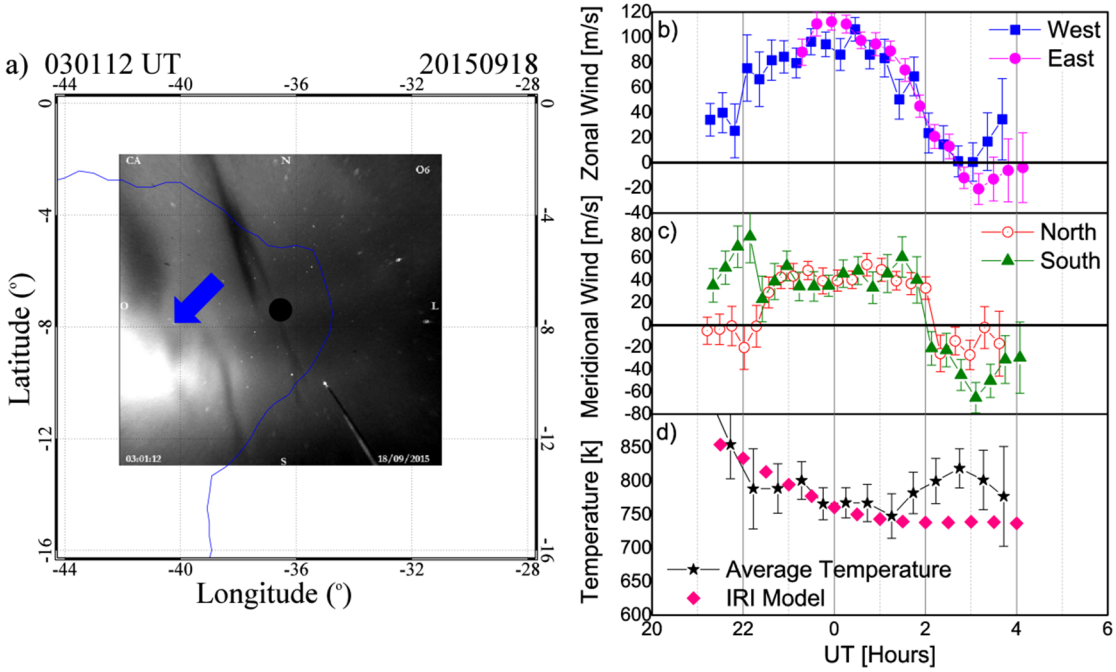

Figure 2 - a) Unwarped OI 630 nm image taken on September 18, 2015, over São João do Cariri (black dot). The blue arrow points to an MBW propagating southwest. Figures b) and c) show the zonal (for west and east look directions) and meridional (for north and south look directions) components of the neutral wind observed by FPI at São João do Cariri. While panel d) shows both the neutral temperature obtained by FPI and the IRI 2016 model.

Discussion

In this section, we analyze the associated ionospheric physical processes in order to explain the EPB/MSTID and EPB/MBW interactions observed at Cachoeira Paulista on September 17-18, 2015.

Four hours before the interactions occurred, an increase in the AE index was observed between 22:00 and 24:00 UT on 09/17/2015, which reached 687 nT. The Kp and Dst indices reached 3- and -10 nT respectively. It is known geomagnetic conditions can interfere in the dynamics of the equatorial ionosphere, generating a disturbance dynamo (Blanc & Richmond, 1980) and consequently changing the propagation direction of the EPB from east to west (e.g., Huang &

Roddy, 2016; Paulino et al., 2010). Huang & Roddy, (2016) observed EPB zonal drift velocity from Communications/Navigation Outage Forecasting System (C/NOFS) satellite data between May 2008 and April 2014 and concluded that the disturbance dynamo is significant in the equatorial region when Kp > 4 or Dst < -60 nT. Therefore, an effect of the disturbance dynamo on the change of EPB direction is unlikely, suggesting that an interaction between MSTID and EPB is a good candidate to explain it.

EPB and MSTID Interaction

The EPBs observed at Cachoeira Paulista, on the early morning of September 18, 2015, propagated toward the northeast. Previous studies in Brazil have shown that plasma bubble drifts from west to east with velocities ranging from 50 to 200 m/s (Paulino et al., 2011; Barros et al., 2018; Pimenta et al., 2003; Sobral et al., 1981). Additionally, the MSTID propagates to the northwest. Nighttime MSTIDs originate mainly in middle latitudes due to the Perkins instability and coupling between E and F regions (Yokoyama & Hysell, 2010). Usually, Northern hemisphere MSTIDs propagate southwestward, while in the Southern hemisphere they propagate to the northwest (Ogawa et al., 2009; Otsuka et al., 2004 and 2007; Shiokawa et al., 2003). For instance, in Brazil, reports of MSTIDs propagating northwestward have been published elsewhere (Amorim et al., 2011; Figueiredo et al., 2018b and references therein).

Previous studies have reported that the EPB can be absorbed by the MSTID when they interact with each other (e.g., Otsuka et al., 2012; Shiokawa et al., 2015). Moreover, these authors suggest that the horizontal shear of the polarization electric field, associated with the MSTID, moved the ambient plasma into the EPB, through magnetic field lines via **E**x**B** drift (Fig. 4 of Otsuka et al., 2012, and Fig. 10b of Shiokawa et al., 2015). In our case, the dark band of the MSTID interacts with the EPB, so the shear between the bright and dark band was not sufficient to fill the EPB depletion.

To explain what physical mechanism was able to grow the EPB along the magnetic field lines, we have used data from ionosonde and magnetometers installed at Cachoeira Paulista. Figure 3 shows (a) the ionospheric parameters from ionograms (h'F, f_oF_2, hmF_2), (b) the zonal electric

206 field, and (c) the vertical drift. Figure 3 (a) shows that during the passage of the dark band
207 MSTID between 02:00 and 03:00 UT, an F layer uplifted was caused by the increase of the
208 eastward electric field (Figure 3(b)). Therefore, the EPB likely grew across the magnetic field
209 lines due to an eastward polarization electric field provided by MSTID and subsequently
210 increased upward **E**x**B** drift of the EPB (Figure e (c)).
211

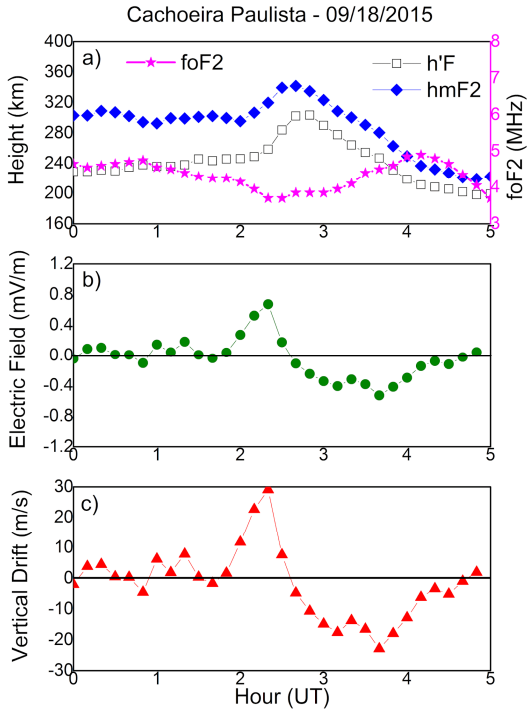

212

213 Figure 3 – a) Ionospheric parameters (h'F, hmF_2, and foF_2) at Cachoeira Paulista on 18/09/2015.
214 b) Zonal electric field calculated using magnetometer. c) Vertical drift profile.
215

216 Figure 4 shows a schematic diagram of the EPB/MSTID interaction between the polarization
217 electric field (δE) and $\delta E \times B$ drift associated with MSTID to explain the physical mechanism
218 that tilts EPB. We can see that the southeastward (northwestward) δE in the dark (bright) airglow
219 region moves the F-region plasma to higher (lower) altitudes via **E**x**B**, resulting in decreases
220 (increases) in the intensity of OI 630 nm airglow (e.g, Shiokawa et al., 2003). The $\delta E \times B$ drift
221 velocity is northeastward (southwestward) in the bright (dark) region. Since the interaction
222 occurs after midnight, the polarization electric field within the EPB is weak and does not cause a
223 plasma drift relative to the plasma ambient (Huang et al., 2010). Thus, southwestward drift

velocity in the dark airglow region due to MSTID may have tilted and it has controlled the west-east drift of the EPB.

In the current event, the thermospheric neutral wind observed by FPI in the southern hemisphere was southwestward during a period when MSTID interacted with EPB. The electric current induced by the neutral wind in the F region in the southern hemisphere is expected to be northwestward. For this case, the polarization electric field generated by Ohm's law in the Southern hemisphere is northwestward (southeastward) in the dark (bright) airglow region. These electric fields cannot maintain the MSTID structures. Therefore, the polarization electric field could be generated mainly in the northern hemisphere, where the electric current was conducive to generating the MSTID polarization electric field (e.g., Otsuka et al., 2004, Otsuka et al., 2012, and Shiokawa et al., 2005).

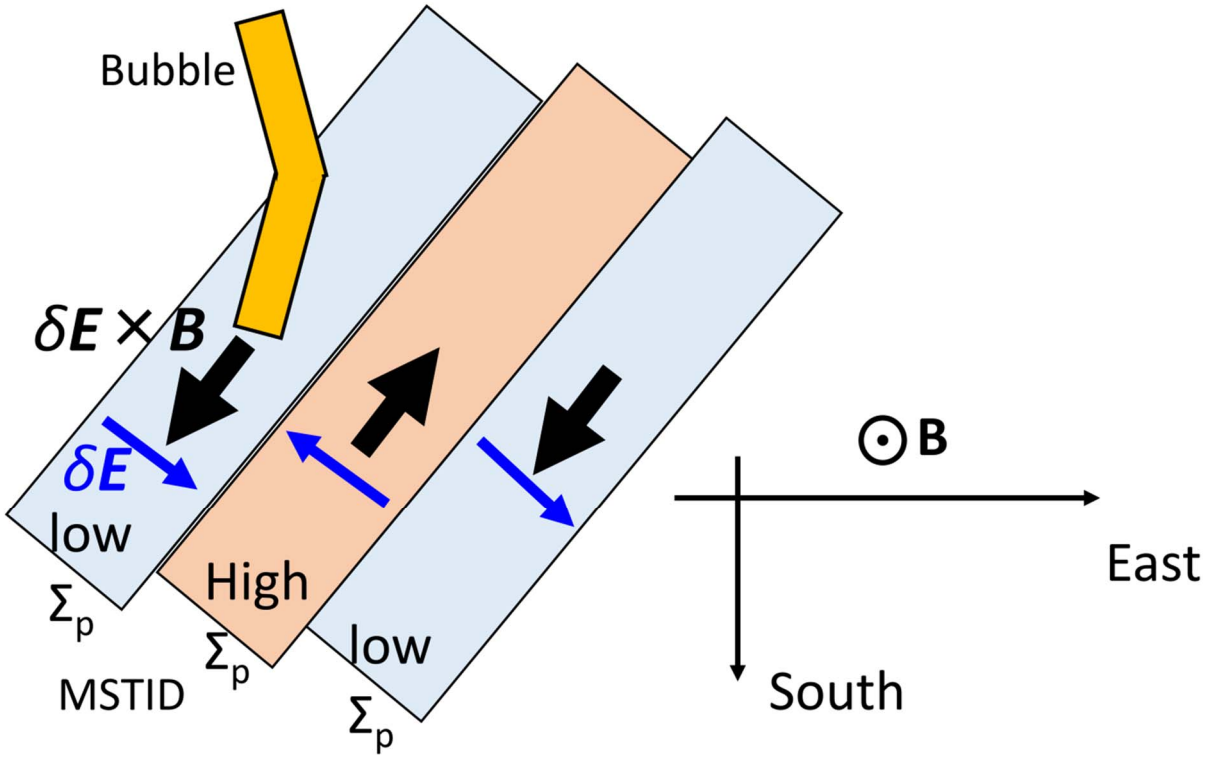

Figure 4 - Schematic upper view diagram of the interaction between MSTID and EPB. The polarization electric field, $\delta \boldsymbol{E}$, of MSTID produces $\delta \boldsymbol{E} \times \boldsymbol{B}$ drift velocities (black arrow). $\delta E \times B$ drift velocities are northeastward (southwestward) in the bright (dark) region. $\sum_P$ is the Pedersen conductivity integrated along the magnetic field line. Bright (dark) regions of MSTID have high (low) Pedersen conductivity. While **B** is the magnetic field out of the page.

A difference between the Otsuka et al. (2012) case and the present result is the duration of the interaction between EPB and MSTID. Otsuka et al. (2012) showed that the EPB disappeared soon after the MSTID interaction, while in the present case, the EPB survived longer. This difference could be due to deeper depletion of plasma density within the EPB and/or a weak polarization electric field shear of the MSTID.

EPB and MBW Interaction

The MBW decreases the F-layer height and increases the critical frequency (foF2). After those alterations, the F region is uplifted by a few kilometers (Figueiredo et al., 2017). The MBW is characterized by an increase of the OI 630 nm airglow intensity, which propagated poleward in both of the hemispheres, and reverses the thermospheric neutral wind direction from equatorward to poleward (Colerico et al., 1996; Herrero & Meriwether, 1980; Otsuka et al., 2003). Therefore, the reverse of neutral wind direction and gravitational diffusion moves the ionospheric plasma from low to middle latitudes along geomagnetic field lines (e.g., Fukushima et al., 2017).

When the observed MBW reached latitudes within the imager's fields of view, it also interacted with the EPB by partially filling the EPB edges with plasma (density and temperature larger than the background plasma) making it brighter even after the MBW had passed. In addition, the MBW does not modify the bubble structure, suggesting that it does not produce a polarization electric field (e.g., MSTID) which absorbs or modifies the structure of the EPB, as noticed in Figure 2a.

Makela et al. (2006) related the occurrence of the EPB and the elongated bands of enhancement in OI 630 nm emission. The authors suggested that this enhancement can be explained by the rapid descent of the F layer associated with winds. Martinis et al. (2009) observed a bright background airglow structure moving toward the South of Arecibo which involved a brighter EPB structure. The authors interpreted this change in the EPB brightness as being mostly due to zonal wind reversal. Krall et al. (2009) used numerical simulation to show that EPB brightness is

generated when the zonal wind stops the **E**x**B** upward drift, increasing the EPB density at the airglow layer.

In the present study, we observed that the interaction between EPB and MBW generates a bright airglow structure at the edge of the EPB as reported by Makela et al. (2006) and Martinis et al. (2009). Also, Figures 2b and 2c show that the MBW reverses directions of the neutral wind components. Based on our present results, we can infer that the brightening mechanism is the same as that suggested by Martinis et al. (2009) and Krall et al. (2009). However, the phenomena responsible for the bright structure of the EPB are different for each of those cases.

The conditions for the EPB development and dissipation after the MSTID and MBW interactions will be the subject of future studies. Further observations and investigations of the electrodynamics, as well as numerical simulations of EPBs, are needed for a better understanding of these phenomena.

Summary and conclusions

Interactions between EPB, MSTID, and MBW were observed at Cachoeira Paulista, Brazil, on the early morning of September 18, 2015, using an all-sky imager for the OI 630 nm emission. As a result of those interactions, the EPBs tilted, grew, and narrowed, but did not disappear. Subsequently, an MBW arose in the equatorial region (7°S) propagating toward a lower latitude (23°S) and also interacting with EPBs over Cachoeira Paulista.

We suggest that the **E**x**B** drift caused by the MSTID allied to a change of the neutral wind due to the MBW, could tilt and control the west-east drift and could fill the EPB with plasma. In addition, the EPB grew along the magnetic field lines suggesting that an eastward polarization electric field from the MSTID provided an eastward polarization electric field to EPB and, consequently, increased the upward **E**x**B** drift of the EPB.

Acknowledgments

The airglow images, magnetometers and digisonde data used in this study were provided by Estudo e Monitoramento BRAsileiro de Clima Espacial — EMBRACE (http://www2.inpe.br/climaespacial/portal/linear-image-video/; http://www2.inpe.br/climaespacial/portal/ionosondes-indexes/; http://www2.inpe.br/climaespacial/portal/index-summary/). We thank Madrigal for the storing and sharing of the scientific data. The wind and neutral temperature data used in this study are freely available for use from the Madrigal database (see http://madrigal.haystack.mit.edu/madrigal/). Please contact Jonathan J. Makela (jmakela@illinois.edu) for further information about those data. The present work was supported by Conselho Nacional de Desenvolvimento Científico e Tecnológico (CNPq), under the processes 470589/2012-4, 305461/2015-0, 303511/2017-6, 307653/2017-0, and 169815/2017-0. C.A.O.B. Figueiredo thanks to the Fundação de Amparo à Pesquisa do Estado de São Paulo (FAPESP) under the process 2018/09066-8. Y. Otsuka and K. Shiokawa thank to JSPS KAKENHI, under the processes JP 15H05815 and JP 16H06286 grants. R.A. Buriti and I. Paulino thanks to the Fundação de Amparo à Pesquisa do Estado da Paraíba by the PRONEX grant. C.A.O.B. Figueiredo thanks to Wayne Hocking and João Marques de Carvalho for improving English writing

References

Abdu, M. A., de Souza, J. R., Kherani, E. A., Batista, I. S., MacDougall, J. W., & Sobral, J. H. A. (2015). Wave structure and polarization electric field development in the bottomside F layer leading to postsunset equatorial spread F. Journal Geophys Res Space Physics, 120:6930–6940. https://doi.org/10.1002/2015JA021235.

Amorim, D. C. M., Pimenta, A. A., Bittencourt, J. A., & Fagundes, P. R. (2011). Long term study of medium-scale traveling ionospheric disturbances using oi 630 nm All-Sky imaging and ionosonde over Brazilian low latitudes. Journal of Geophysical Research, 116, A06312. https://doi.org/10.1029/2010JA016090

Barros, D., Takahashi, H., Wrasse, C. M., & Figueiredo, C. A. O. B. (2018). Characteristics of equatorial plasma bubbles observed by TEC map based on ground-based GNSS receivers

over South America. Annales Geophysicae, 36(1), 91–100. https://doi.org/10.5194/angeo-36-91-2018

Blanc, M., & Richmond, A. (1980). The ionospheric disturbance dynamo, *Journal of Geophysical Research*, 85(A4), 1669– 1686, doi:10.1029/JA085iA04p01669.

Burnside, R., Herrero, F., Meriwether, J., &Walker, J. (1981). Optical observations of thermospheric dynamics at Arecibo, J. Geophys. Res.-Space, 86, 5532–5540.

Clemesha, B.R. (1964). An investigation of the irregularities in the F-region associated with equatorial type spread-F. Journal of Atmospheric and Terrestrial Physics 26, 91–122.

Colerico, M., Mendillo, M., Nottingham, D., Baumgardner, J., Meriwether, J., Mirick, J., Reinisch, B. W., Scali, J. L., Fesen, C.G., & Biondi, M.A. (1996). Coordinated measurements of F region dynamic related to the thermospheric midnight temperature maximum. J Geophys Res 101:26783–26793

Farley, D. T., Bonelli, E., Fejer, B. G., & Larsen, M. F. (1986). The prereversal enhancement of the zonal eletric field in the equatorial ionosphere. Journal of Geophysical Research, v. 86, n. A12, p. 13723–13728.

Figueiredo, C. A. O. B., Buriti, R. A., Paulino, I., Meriwether, J. W., Makela, J. J., & Batista, I. S., et al. (2017). Effects of the midnight temperature maximum observed in the thermosphere–ionosphere over the northeast of Brazil. Annales de Geophysique, 35, 953–963. https://doi.org/10.5194/angeo-35-953-2017

Figueiredo, C. A. O. B., Takahashi, H., Wrasse, C. M., Otsuka, Y., Shiokawa, K., & Barros, D. (2018a). Medium-scale traveling ionospheric disturbances observed by detrended total electron content maps over Brazil. Journal of Geophysical Research: Space Physics, 123, 2215–2227. https://doi.org/10.1002/2017JA025021

Figueiredo, C. A. O. B., Takahashi, H., Wrasse, C. M., Otsuka, Y., Shiokawa, K., & Barros, D. (2018b). Investigation of nighttime MSTIDS observed by optical thermosphere imagers at low latitudes: Morphology, propagation direction, and wind filtering. Journal of Geophysical Research: Space Physics, 123, 7843–7857. https://doi.org/10.1029/2018JA025438.

Bilitza, D., Altadill, D., Truhlik, V., Shubin, V., Galkin, I., Reinisch, B., & Huang, X. (2017). International Reference Ionosphere 2016: From ionospheric climate to real-time weather predictions, Space Weather, 15, 418-429, doi:10.1002/2016SW001593.

Fukushima, D., Shiokawa, K., Otsuka, Y., Kubota, M., Yokoyama, T., Nishioka, M. et al. (2017). Geomagnetically conjugate observations of ionospheric and thermospheric variations accompanied by a midnight brightness wave at low latitudes. Earth Planets Space 69:112. doi:10.1186/s40623-017-0698-z

Haerendel, G. (1973). Theory of equatorial spread-F, Report Max-Planck Institute.

Herrero, F.A., & Meriwether, J.W. (1980). 6300-Å airglow meridional intensity gradients. J Geophys Res 85:4194–4204

Herrero, F., Spencer, N., & Mayr, H. (1993). Thermosphere and F-region plasma dynamics in the equatorial region, Adv. Space Res., 13, 201–220, 1993.

Hines, C. O. (1960). Internal atmospheric gravity waves at ionospheric heights. Canadian Journal of Physics, 38(11), 1441–1481. https://doi.org/10.1139/p60-150

Hooke, W. H. (1968). Ionospheric irregularities produced by internal atmospheric gravity waves. Journal of Atmospheric and Terrestrial Physics, 30(5), 795–823. https://doi.org/10.1016/S0021-9169(68)80033-9

Huang, C. S., & Roddy, P. A. (2016). Effects of solar and geomagnetic activities on the zonal drift of equatorial plasma bubbles, J. Geophys. Res. Space Physics, 121, 628– 637, doi:10.1002/2015JA021900

Hunsucker, R. D. (1982). Atmospheric gravity waves generated in the high-latitude ionosphere: A review. Reviews of Geophysics, 20, 293–315. https://doi.org/10.1029/RG020i002p00293

Kelley, M. C. (2009). The Earth's Ionosphere, Elsevier.

Kelley, M. C., & Miller, C. A. (1997). Electrodynamics of midlatitude spread F: 3. Electrohydrodynamic waves? A new look at the role of electric fields in thermospheric wave dynamics, J. Geophys. Res., 102, 11,539–11,547.

Krall, J., Huba, J. D., & Martinis, C. R. (2009). Three-dimensional modeling of equatorial spread F airglow enhancements, Geophys. Res. Lett., 36, L10103, doi:10.1029/2009GL038441.

Krall, J., Huba, J. D., Ossakow, S. L., Joyce, G., Makela, J. J., Miller, E. S., & Kelley, M. C. (2011). Modeling of equatorial plasma bubbles triggered by non-equatorial traveling ionospheric disturbances, Geophys. Res. Lett., 38, L08103, doi:10.1029/2011GL046890.

Link, R., & Cogger, L. (1988) A reexamination of the OI 6300 Å nightglow, J. Geophys. Res.-Space, 93, 9883–9892.

Martinis, C., Baumgardner, J., Mendillo, M., Su, S.-Y., & Aponte, N. (2009). Brightening of 630.0 nm equatorial spread-F airglow depletions, J. Geophys. Res., 114, A06318, doi:10.1029/2008JA013931.

Makela, J. J., Kelley, M. C., & Nicolls, M. J. (2006). Optical observations of the development of secondary instabilities on the eastern wall of an equatorial plasma bubble, J. Geophys. Res., 111, A09311, doi:10.1029/2006JA011646.

Makela, J. J., Meriwether, J. W., Lima, J. P., Miller, E. S., & Armstrong, S. J. (2009). The remote equatorial nighttime observatory of ionospheric regions project and the international heliospherical year, Earth Moon Planets, 104, 211–226.

Meriwether, J., Makela, J., Huang, Y., Fisher, D., Buriti, R., Medeiros, A., & Takahashi, H. (2011). Climatology of the nighttime equatorial thermospheric winds and temperatures over Brazil near solar minimum, J. Geophys. Res.-Space, 116, A04322,

Mesquita, R. L. A., Meriwether, J. W., Makela, J. J., Fisher, D. J., Harding, B. J., Sanders, S. C., Tesema, F., & Ridley, A. J. (2018). New results on the mid-latitude midnight temperature maximum, Ann. Geophys., 36, 541-553, https://doi.org/10.5194/angeo-36-541-2018.

Miller, C. A., Swartz, W. E. , Kelley, M. C., Mendillo, M. , Nottingham, D. , Scali, J., & Reinisch, B. (1997). Electrodynamics of midlatitude spread F: 1. Observations of unstable, gravity wave-induced ionospheric electric fields at tropical latitudes, J. Geophys. Res., 102, 11,521–11,532.

Miller, E. S., Makela, J. J., & Kelley, M. C. (2009). Seeding of equatorial plasma depletions by polarization electric fields from middle latitudes: Experimental evidence, Geophys. Res. Lett., 36, L18105, doi:10.1029/2009GL039695.

Narayanan, V. L., Gurubaran, S., Shiokawa, K., & Emperumal, K. (2016). Shrinking equatorial plasma bubbles, J. Geophys. Res. Space Physics, 121, 6924–6935, doi:10.1002/2016JA022633.

Ogawa, T., Nishitani, N., Otsuka, Y., Shiokawa, K., Tsugawa, T., & Hosokawa, K. (2009). Medium-scale traveling ionospheric disturbances observed with the SuperDARN Hokkaido radar, all-sky imager, and GPS network and their relation to concurrent sporadic E irregularities, J. Geophys. Res., 114, A03316, doi:10.1029/2008JA013893.

425 Otsuka, Y., Kadota, T., Shiokawa, K., Ogawa, T., Kawamura, S., Fukao, S., Zhang, S. R. (2003).
426 Optical and radio measurements of a 630-nm airglow enhancement over Japan on 9
427 September 1999. J Geophys Res 102(A6):1252. doi: 10.1029/2002JA009594
428 Otsuka, Y., K. Shiokawa, T. Ogawa, and P. Wilkinson (2004). Geomagnetic conjugate
429 observations of medium-scale traveling ionospheric disturbances at midlatitude using all-
430 sky airglow imagers, Geophys. Res. Lett., 31, L15803, doi:10.1029/2004GL020262.
431 Otsuka, Y., F. Onoma, K. Shiokawa, T. Ogawa, M. Yamamoto, & S. Fukao (2007).
432 Simultaneous observations of nighttime medium-scale traveling ionospheric disturbances
433 and E region field-aligned irregularities at midlatitude, J. Geophys. Res., 112, A06317,
434 doi:10.1029/2005JA011548.
435 Otsuka, Y., Shiokawa, K., & Ogawa, T. (2012). Disappearance of equatorial plasma bubble after
436 interaction with mid-latitude medium-scale traveling ionospheric disturbance, Geophys.
437 Res. Lett., 39, L14105, doi:10.1029/2012GL052286.
438 Paulino, I., Takahashi, H., Medeiros, A.F., Wrasse, C.M., Buriti, R.A., Sobral, J.H.A., &
439 GOBBI, D. (2011). Plasma bubble zonal drift characteristics observed by airglow images
440 over Brazilian tropical region. Revista Brasileira de Geofísica, 29(2), 239-246. DOI:
441 10.1590/S0102-261X2011000200003
442 Paulino, I. , Medeiros, A.F., Buriti, R.A., Sobral, J.H.A., Takahashi, H., & Gobbi, D. (2010).
443 Optical observations of plasma bubble westward drifts over Brazilian tropical region,
444 Journal of Atmospheric and Solar-Terrestrial Physics, Volume 72, Issues 5–6, Pages 521-
445 527, ISSN 1364-6826.
446 Pimenta, A., Bittencourt, J., Fagundes, P., Sahai, Y., Buriti, R., Takahashi, H., & Taylor, M. J.
447 (2003). Ionospheric plasma bubble zonal drifts over the tropical region: a study using oi
448 630nm emission all-sky images. Journal of Atmospheric and Solar-Terrestrial Physics, v.
449 65, n. 10, p. 1117–1126.
450 Rishbeth, H. (2000). The equatorial F-layer: progress and puzzles, Annales Geophysicae,
451 Springer, 18, 730–739.
452 Shiokawa, K., Otsuka, Y., Ihara, C., Ogawa, T., & Rich, F. J. (2003). Ground and satellite
453 observations of nighttime medium-scale traveling ionospheric disturbance at midlatitude,
454 J. Geophys. Res., 108(A4), 1145, doi:10.1029/2002JA009639.

455 Shiokawa, K., Otsuka, Y., Lynn, K. J. W., Wilkinson, P., & Tsugawa, T. (2015). Airglow-
456 imaging observation of plasma bubble disappearance at geomagnetically conjugate
457 points, Earth Planets Space, 67, 43, doi:10.1186/s40623-015-0202-6.
458 Sobral, J.H.A., Abdu, M.A., Batista, I.S., & Zamlutti, C.J. (1980). Association between plasma
459 bubble irregularities and emission disturbance over Brazilian low latitudes. Geophysical
460 Research Letters, 11, 980–982.
461 Takahashi, H., Wrasse, C.M., Otsuka, Y., Ivo, A., Gomes, V., Paulino, I., Medeiros, A.F.,
462 Denardini, C.M., Sant'Anna, N., & Shiokawa, K. (2015). Plasma bubble monitoring by
463 TEC map and 630nm airglow image, Journal of Atmospheric and Solar-Terrestrial
464 Physics, Volumes 130–131, https://doi.org/10.1016/j.jastp.2015.06.003.
465 Takahashi, H., Wrasse, C. M., Figueiredo, C. A. O. B., Barros, D., Abdu, M. A., Otsuka, Y., &
466 Shiokawa, K. (2018). Equatorial plasma bubble seeding by MSTIDs in the ionosphere.
467 Progress in Earth and Planetary Science, 5(1), 32. https://doi.org/10.1186/s40645-018-
468 0189-2
469 Tsunoda, R.T. (2010). On seeding equatorial spread F: circular gravity waves. Geophysical
470 Research Letters 37, L10 104.
471 Vadas, S.L., Taylor, M.J., Pautet, P.D., Stamus, P.A., Fritts, D.C., Liu, H.L., Sao Sabbas, F.T.,
472 Rampinelli, V.T., Batista, P., & Takahashi, H., 2009. Convection: the likely source of the
473 medium-scale gravity waves observed in the OH airglow layer near Brasilia, Brazil,
474 during the SpreadFEx campaign. Annales Geophysicae 27, 231–259.
475 Woodman, R.F., & LaHoz, C. (1976). Radar observations of F region equatorial irregularities.
476 Journal of Geophysical Research 81, 20.
477 Yokoyama, T., & Hysell, D. L. (2010). A new midlatitude ionosphere electrodynamics coupling
478 model (MIECO): Latitudinal dependence and propagation of medium-scale traveling
479 ionospheric disturbances. Geophysical Research Letters, 37, L08105.
480 https://doi.org/10.1029/2010GL042598

Figure 1.

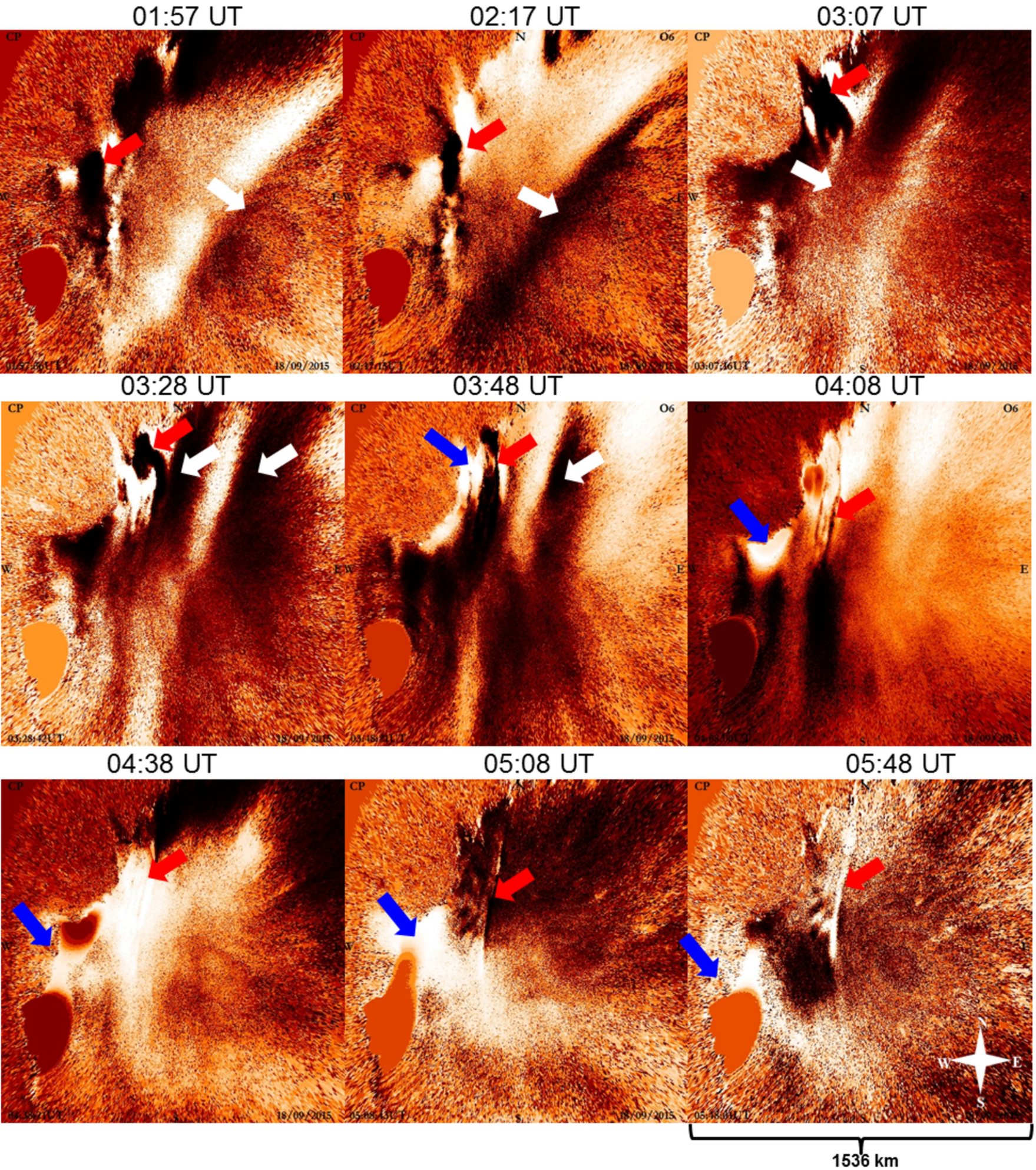
01:57 UT
02:17 UT
03:07 UT
03:28 UT
03:48 UT
04:08 UT
04:38 UT
05:08 UT
05:48 UT
CP
O6
N
E
W
S
18/09/2015
1536 km
1536 km

Figure 2.

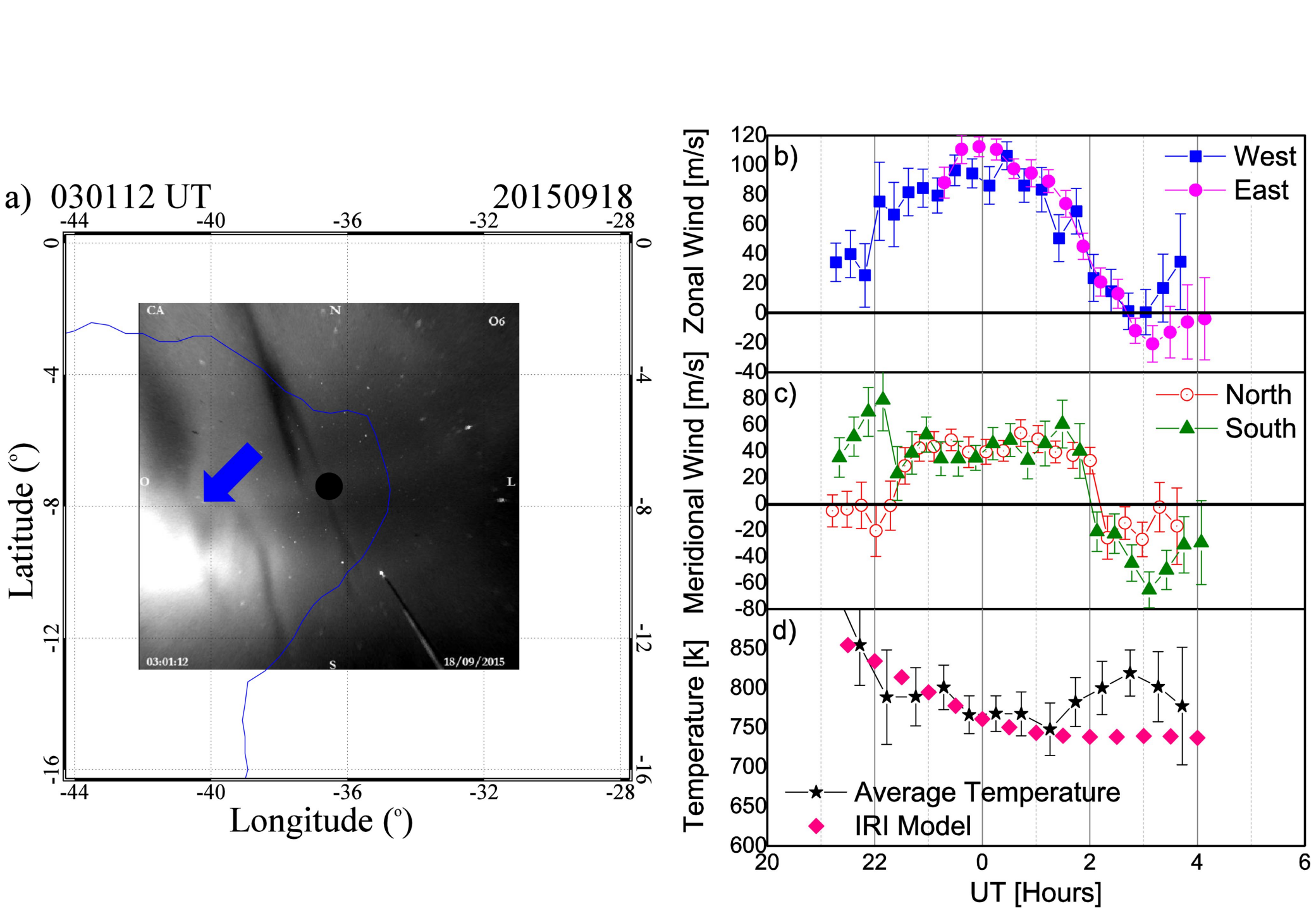
a) 030112 UT
20150918
-44
-40
-36
-32
-28
0
-4
-8
-12
-16
Latitude (°)
Longitude (°)
CA
N
O6
O
L
S
03:01:12
18/09/2015
b)
West
East
Zonal Wind [m/s]
c)
North
South
Meridional Wind [m/s]
d)
Average Temperature
IRI Model
Temperature [k]
UT [Hours]

Figure 3.

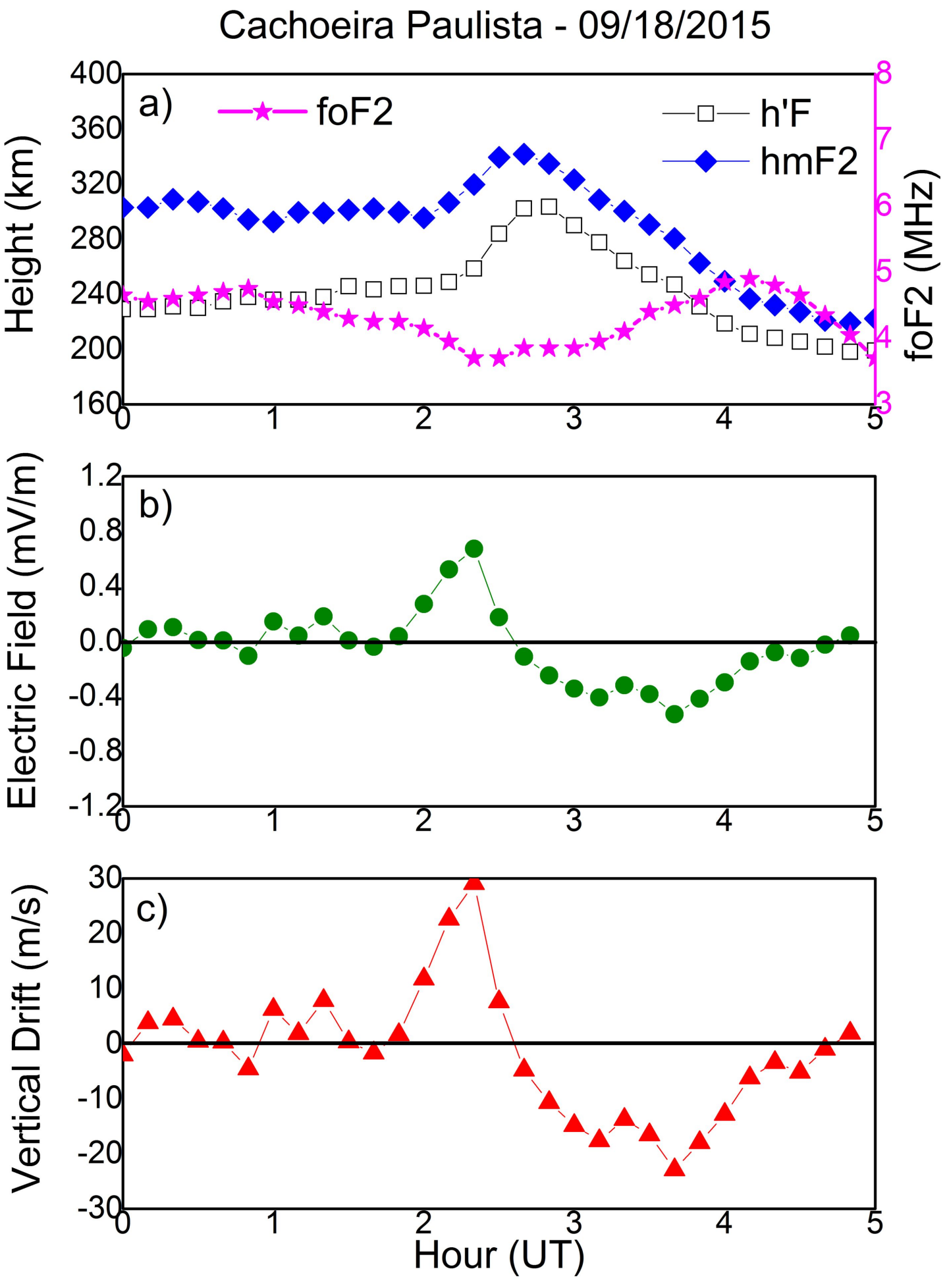
Cachoeira Paulista - 09/18/2015
a)
foF2
h'F
hmF2
Height (km)
foF2 (MHz)
400
360
320
280
240
200
160
8
7
6
5
4
3
0
1
2
3
4
5
b)
Electric Field (mV/m)
1.2
0.8
0.4
0.0
-0.4
-0.8
-1.2
c)
Vertical Drift (m/s)
30
20
10
0
-10
-20
-30
Hour (UT)

Figure 4.

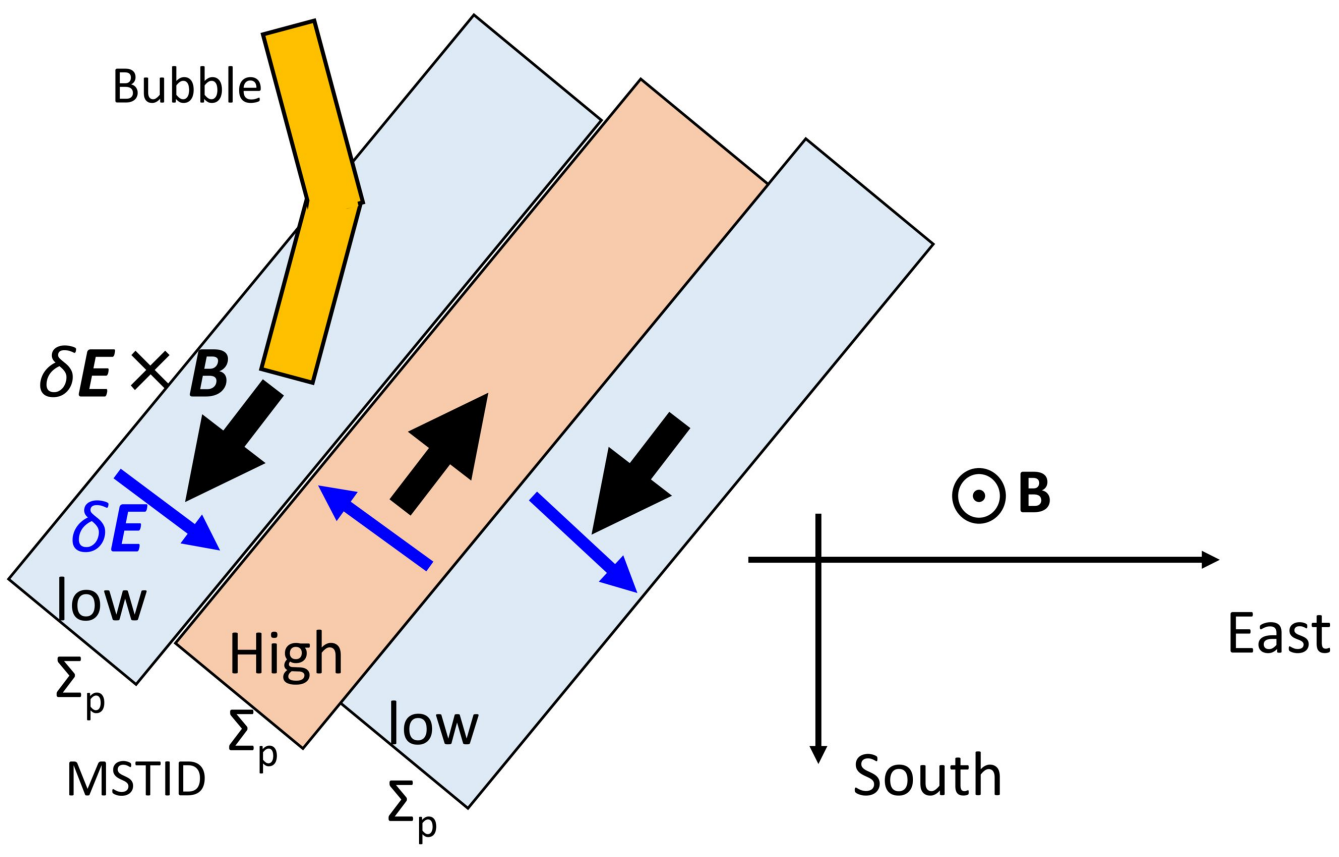
Bubble
δE × B
δE
low
Σp
High
Σp
low
Σp
MSTID
⊙B
East
South